COMPUTER SIMULATION OF FLAGELLAR MOVEMENT

I. Demonstration of Stable Bend Propagation and Bend Initiation by the Sliding Filament Model

C. J. BROKAW

From the Division of Biology, California Institute of Technology, Pasadena, California 91109

ABSTRACT A program has been developed for digital computer simulation of the movement of a flagellar model consisting of straight segments connected by joints at which bending occurs. The program finds values for the rate of bending at each joint by solving equations which balance active, viscous, and elastic bending moments at each joint. These bending rates are then used to compute the next position of the model. Stable swimming movements, similar to real flagellar movements, can be generated routinely with a 25-segment model using 16 time steps/beat cycle. These results depend on four assumptions about internal flagellar mechanisms: (*a*) Bending is generated by a sliding filament process. (*b*) The active process is controlled locally by the curvature of the flagellum. (*c*) Nonlinear elastic resistances stabilize the amplitude of the movement. (*d*) Internal viscous resistances stabilize the wavelength of the movement and explain the relatively low sensitivity of flagellar movement to changes in external viscosity.

INTRODUCTION

The movements of flagella and cilia require not only a mechanochemical mechanism for bending, but also a mechanism to control the propagation and rhythmic initiation of bends. A control mechanism for bending wave propagation, based on a "sliding filament" process for the generation of bending, has been presented in a previous paper (Brokaw, 1971). It was suggested that control of the local magnitude of the active sliding process by the local curvature of the filaments would establish a feedback loop which could be responsible for the rhythmic propagation of bending waves. This combination of a simple control relationship with a sliding filament model for the active process appears to resolve the difficulties encountered with earlier suggestions for the control of bend propagation, which were based on a "local bending" model for the active process.

The sliding filament model for flagella has now been examined further by con-

struction of a working model which incorporates the suggested control process. The model has not been constructed in the real, mechanical sense, but in the form of a computer program which can be used to simulate the movement of the model on a digital computer.

The computer model is developed from the following assumptions:

(*a*) The active bending moment generated within a flagellum results from an active sliding process, which is locally controlled by the curvature of the flagellum. Using equations and notation from Brokaw (1971), this assumption can be represented by an equation,

$$dM_a/ds = -m(\kappa). \tag{1}$$

The curvature $d\theta/ds$ of a flagellum at any point s along its length is represented by κ; the function $\kappa(s)$ describes the shape of the flagellum at any time, and a function $\kappa(s, t)$ completely describes the bending movements of the flagellum. The active bending moment at any point along the length of the flagellum is represented by M_a, and the local magnitude of the active sliding process is represented by m, which is a measure of active moment generated per unit length.

Equation 1 incorporates the basic assumptions about the sliding filament mechanism for bending and the control of bending, which are being tested by the model. The computer model is in other respects, however, a general purpose model which can incorporate other mechanisms for the control of M_a, as illustrated in Appendix II.

Equation 1 is independent of any detailed specifications about the number and location of filaments within flagella, and these details will not be examined in the present paper. It will be assumed, however, that the internal organization of a flagellum restricts its bending to a single plane, and only planar bending of the model will be considered in this paper.

(*b*) The filaments between which active sliding occurs are assumed to be rigidly tied together at the base of the flagellum, so that no interfilament shear occurs at the base of the flagellum. This is a reasonable interpretation of the observations of Satir (1965, 1968). The consequences of this assumption will be examined in future work.

(*c*) The filaments between which sliding occurs are considered to be completely incompressible and inextensible, so that there is a simple relationship between bending of a flagellum and shear between its filaments.

(*d*) The flagellum is represented by a model which consists of a connected series of straight segments of equal length. Bending of the model occurs only at the "joints" between the segments. This approximation is basic to the process of simulating the movement of a flagellum by digital computation. The accuracy of this approximation can be evaluated by comparing the results obtained from computations with different numbers of segments.

(*e*) The external viscous forces acting on a flagellum as it moves through a viscous medium are obtained using the approximate method introduced by Gray and Hancock (1955). If F_N and F_L are normal and longitudinal forces in the flagellum, resulting from the external viscous forces,

$$\begin{aligned} dF_N &= -C_N V_N \, ds, \\ dF_L &= -C_L V_L \, ds. \end{aligned} \tag{2}$$

C_N and C_L are normal and tangential drag coefficients for movement of a thin filament through a viscous medium with normal and tangential velocities V_N and V_L. The drag coefficients are assumed to be constant over the length of the flagellum. Additional assumptions involved in this approximation are discussed by Brokaw (1970). In accordance with earlier work, a value of 1.8 has been used for the ratio C_N/C_L throughout the work described in this paper.

A more exact analysis of the hydrodynamics of a moving flagellum could be carried out using the relationships developed by Cox (1970) for comparison with the results obtained with the method of Gray and Hancock. Although this has not yet been done, some validation of the approximate method has been obtained from its success in predicting the swimming velocities of sperm flagella (Gray and Hancock, 1955; Brokaw, 1965, 1970).

DEVELOPMENT OF THE MODEL

The control problem solved by a flagellum may be considered to be the generation of the proper amount of active bending moment M_a to balance the moments which resist bending of the flagellum. The most important bending resistance is probably that which results from the external viscosity of the surrounding medium, since this is the resistance against which a flagellum does biologically useful work. The starting point for this analysis is therefore an equation for the balance between viscous and active bending moments, along the entire length of the flagellum:

$$M_v(s) = -M_a(s) \qquad \text{for } 0 \leq s \leq 1. \tag{3}$$

The length of the flagellum is used as a unit length. The sign conventions, as in Brokaw (1971), are such that a positive moment is one which tends to cause positive curvature of the flagellum.

M_v represents the viscous bending moment imposed on a flagellum by moving against the viscous resistance of the external medium. A method has been developed (Brokaw, 1970) to obtain $M_v(s)$ by numerical integration for any form of planar bending movement, starting from the assumptions contained in equation 2. In that method, the velocities V_N and V_L are obtained from a double integration along s involving $\kappa(s)$ and $\dot{\kappa}(s) \equiv d\kappa(s)/dt$, which describe the form and bending behavior of the flagellum at any time. V_N and V_L also depend on the initial values

of angular velocity (W) and linear velocities (V_x and V_y) at the basal end of the flagellum. dF_N and dF_L are then obtained from equation 2, and M_s is obtained after two further integrations along s. If the values of W, V_x, and/or V_y are unknown, they can be obtained by setting up equations which satisfy boundary conditions for force and moment at the ends of the flagellum.

In simulating the movement of the model, boundary conditions and an initial distribution of $\kappa(s)$ are specified, but $\dot{\kappa}(s)$ is unknown. Equation 3 must be solved to obtain $\dot{\kappa}(s)$. These values of $\dot{\kappa}(s)$ are then used to find a new distribution of $\kappa(s)$, by using the following approximation:

$$\kappa(s, t + \delta t) = \kappa(s, t) + \dot{\kappa}(s, t)\delta t + \frac{1}{2}[\dot{\kappa}(s, t) - \dot{\kappa}(s, t - \delta t)]\delta t. \qquad (4)$$

The process is then repeated, using $\kappa(s, t + \delta t)$ to describe the shape of the flagellum. This procedure generates a function $\kappa(s, t)$ which represents the movement of the model. The movement can be examined by plotting x, y values obtained by a double integration of $\kappa(s)$ to obtain images of the shape of the flagellar model at selected times.

If the flagellar model contains n straight segments, $n - 1$ unknown values of $\dot{\kappa}(s)$, corresponding to the rate of bending at each of the joints between the straight segments, must be computed. Using j and k as integer variables to represent the positions of the joints along the length of the model, $n - 1$ expressions for M_s at each joint can be obtained in the following form:

$$M_s(j) = \sum_{k=1}^{j-1} A(j, k)\dot{\kappa}(k) + A(j, n)W + A(j, n + 1)V_x + A(j, n + 2)V_y. \qquad (5)$$

The A coefficients in equation 5 are obtained by integration of functions of $\kappa(s)$, C_N, and C_L, using methods similar to those used previously (Brokaw, 1970). These coefficients are described in greater detail in Appendix I.

At each joint, an expression for M_a is also obtained. For the case where the magnitude of the active process is a linear function of the curvature, as discussed in the earlier paper (Brokaw, 1971), we can write $m(\kappa) = -m_0\kappa$, where m_0 is a constant. Then, a discrete form of equation 1 is:

$$M_a(j) = M_a(j - 1) + m_0[\kappa(j) + \kappa(j - 1)]/2n, \qquad (6)$$

which leads to

$$M_a(j) = M_0 - B(j), \qquad (7)$$

where

$$B(j) = -\sum_{k=1}^{j} m_0[\kappa(k) + \kappa(k - 1)]/2n, \qquad [\kappa(0) \equiv 0] \qquad (8)$$

and M_0 represents shear moment between the filaments at the base of the flagellum.

Insertion of these expressions into equation 3 now provides $n - 1$ equations which balance the active and viscous bending moments at each joint:

$$M_v(j) + A(j, n + 3)M_0 = B(j) \qquad \text{for } 1 \leq j \leq n - 1, \tag{9}$$

where

$$A(j, n + 3) = 1 \qquad \text{for } 1 \leq j \leq n - 1. \tag{10}$$

This set of $n - 1$ simultaneous linear equations can now be solved to determine the $n - 1$ unknown values of $\dot{\kappa}(k)$, if the values of W, V_x, V_y, and M_0 are known. In general, these four quantities will not be known, so that four additional equations are required which satisfy boundary conditions at the ends of the model.

Only the case of a free-swimming flagellum, without a head or cell body, will be considered in this paper. With such a flagellum, there are no external forces or moments at the ends of the flagellum. In the equations (Appendix I) for integrating the forces and moment resulting from external viscous forces, the forces and moment applied to the basal end of the model are 0. At the distal end of the model, these boundary conditions then provide three additional equations:

$$M_v(n) = 0, \tag{11}$$

$$F_x(n) = 0, \tag{12}$$

$$F_y(n) = 0. \tag{13}$$

$F_x(n)$ and $F_y(n)$ represent the x and y components of any external force applied to the distal end of the model. The expressions on the left of these three equations can be written in the form of equation 5, using $A(n, k)$ coefficients for equation 11, $A(n + 1, k)$ coefficients for equation 12, and $A(n + 2, k)$ coefficients for equation 13.

If the filaments within a flagellum can slide freely past each other at the distal end of the flagellum, the final boundary condition equation must be:

$$M_a(n) = 0, \tag{14}$$

or

$$A(n + 3, n + 3)M_0 = B(n + 3), \tag{15}$$

where $A(n + 3, n + 3) = 1$, and $B(n + 3)$ is obtained from equation 8 with $j = n$.

A finite value of M_0 may appear to be inconsistent with equation 3 and the condition that $M_v = 0$ at the base of the model; however, if the flagellar filaments are firmly tied together at the base, the first segment of the model effectively contains

a very high shear resistance, which absorbs all the internal shear moment generated along the model. The result is that the internal shear moment, which is approximately equal to M_0 at $j = 1$, actually falls to 0 at the basal end of the model.

An $n + 3$ by $n + 3$ matrix of $A(j, k)$ coefficients and a set of $n + 3$ values of $B(j)$ have now been obtained, which can be solved to determine the $n + 3$ unknown quantities which describe the movement of the model. In its present form, the model contains only two adjustable parameters which can determine the movement: C_N/C_L, which describes the viscous environment, and m_0/C_L, which measures the magnitude of the active process relative to the viscosity of the medium. No stable solutions have been found with this form of the model. The model will now be expanded to include five additional internal parameters: a time delay in the active process, and four internal resistances to bending.

Time Delay in the Active Process

It is unlikely that any control mechanism for the active process can respond instantaneously to changes in curvature. A time delay in the control process will cause a phase shift such that the variations in m will lag slightly behind the variations in $-\kappa$, and as a consequence, the variation in $-M_a$ will lag slightly behind the variation in M_v. As suggested previously (Brokaw, 1971), this will allow some of the active bending moment to vary in phase with the bending moment resulting from elastic properties of the flagellum, so that these elastic bending moments can also be balanced by the active bending moment.

A time delay in the control process can be inserted into the model by using in equations 6 and 8 the values of $\kappa(j)$ and $\kappa(j - 1)$ at an earlier time, rather than the current values. The magnitude of the time delay inserted in this manner will be represented by τ.

Internal Elastic Bending Resistance

The aggregate elastic bending resistance of the individual filaments and other structures within the flagellum will be represented by E_B. E_B is equivalent to the quantity $2\alpha_0$ used previously to represent the elastic bending resistance of a two-filament model (Brokaw, 1966 *a*, 1971). If the moment M_e resulting from elastic bending resistance is included, equation 3 becomes

$$M_v = -M_a - M_e, \tag{16}$$

where

$$M_e = -E_B\kappa. \tag{17}$$

This is incorporated into the system of equations by modifying the values of $B(j)$:

$$B(j) = B(i) + E_B\kappa(j), \qquad \text{for } 1 \leq j \leq n-1. \tag{18}$$

No modification of the boundary-condition equations is required.

Internal Viscous Bending Resistance

The internal viscous bending resistance is one which generates an additional viscous bending moment equal to $-C_B\dot{\kappa}(j)$ at each joint. C_B is a coefficient of internal bending viscosity. This is incorporated into the system of equations by:

$$A(j,j) = -C_B \qquad \text{for } 1 \leq j \leq n-1. \tag{19}$$

No modification of the boundary condition equations is required. The values of $A(j,j)$ resulting from the consideration of external viscous resistances by the methods given in Appendix I are all 0.

Internal Elastic and Viscous Shear Resistances

The internal shear resistances influence M_0 as well as the balance of moments at each joint. Equation 15 must be modified, but the other boundary condition equations are unchanged.

Let M_s represent the bending moment resulting from shearing forces between the filaments. In the absence of internal shear resistances, M_s is equivalent to M_a. When internal shear resistances are present,

$$dM_s/ds = -m + E_S\sigma + C_S\dot{\sigma}. \tag{20}$$

σ is a dimensionless measure of longitudinal shear within a flagellum at a point s. It is equal to the angle (in radians) of bend between s and a point where there is no internal shear, in this case, the base of the flagellum. In the two-filament model used previously (Brokaw, 1971), the shear displacement between two filaments separated by a distance r was represented by u, and $u = r\sigma$. The shear rate $d\sigma/dt$ is represented by $\dot{\sigma}$. E_s is a measure of the elastic shear resistance, equivalent to $r^2\alpha_2$ of the previous two-filament model, and C_S is a measure of viscous shear resistance.

If no shear is allowed in the basal segment of the flagellar model, the shear in the jth segment of the-model is given by:

$$\sigma(j) = (1/n)\sum_{i=2}^{j}\kappa(i-1), \qquad \text{for } 2 \leq j \leq n-1, \tag{21}$$

and the rate of shear in the jth segment is given by:

$$\dot{\sigma}(j) = (1/n)\sum_{i=2}^{j}\dot{\kappa}(i-1) \qquad \text{for } 2 \leq j \leq n-1. \tag{22}$$

After integration of equation 20, M_s can be used in place of M_a in the equations for the balance of moments at each joint. This leads to the following modifications of the coefficients for the set of equations:

$$B(j) = B(j) - (1/n^2) \sum_{k=2}^{j} E_S \sum_{i=2}^{k} \kappa(i-1), \qquad \text{for } 2 \leq j \leq n-1, \tag{23}$$

and

$$A(j, k) = A(j, k) + (j-k)C_S/n^2, \qquad \text{for } 1 \leq k \leq j-1 \text{ and } 1 \leq j \leq n-1. \tag{24}$$

The $n+3$rd equation must also be modified so that

$$M_s(n) = 0, \tag{25}$$

instead of equation 14, so that equation 15 is replaced by:

$$\sum_{k=1}^{n-1} A(n+3, k)\dot{\kappa}(k) + A(n+3, n+3)M_0 = B(n+3), \tag{26}$$

where

$$A(n+3, k) = (n-k)C_S/n^2, \qquad \text{for } 1 \leq k+n-1, \tag{27}$$

and

$$B(n+3) = -(m_0/2n) \sum_{k=1}^{n} [\kappa(k) + \kappa(k-1)] - (1/n^2) \sum_{k=2}^{n} E_S \sum_{i=2}^{k} \kappa(i-1). \tag{28}$$

Solutions to this modified set of $n+3$ equations have been computed with a library routine which uses a straightforward pivot condensation with row interchange, followed by back-substitution.

RESULTS

Fig. 1 shows the shape of the flagellar model at selected times in a computer simulation experiment which covered a time period equal to six beat cycles. The model was initially given the shape shown in position 1. After two to three beat cycles, the transient effects of the initial position have nearly disappeared, and the model approaches a stable, periodic movement which can be continued until a computing time limit is reached. The stable movement pattern is independent of the initial state, but in its present form the model will not start from a completely straight position. A slight modification of the model, such that the values of curvature for

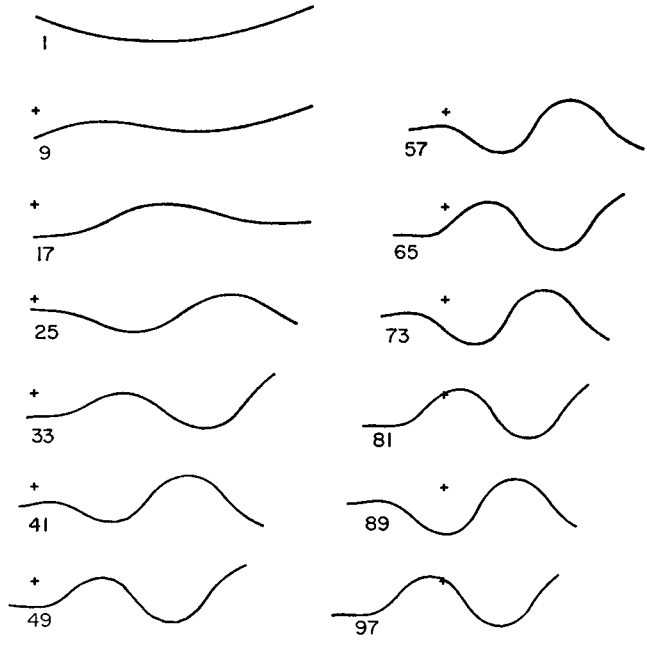

FIGURE 1 Configurations of a flagellar model from an extended movement simulation run. Each image is identified by a number which equals 1 + the number of time integration steps performed according to equation 4; there are eight time steps, or ½ beat cycle, between each successive image. Each image is positioned relative to a small cross which locates the initial position of the basal end of the model. The parameters used for this computation are listed in Table I.

which $m(\kappa) = 0$ are different from those for which the elastic bending moment is 0, would allow the model to start from a completely straight position, as well as any other position.

The parameters used to obtain the movement illustrated in Fig. 1 are listed in Table I. The numerical parameters for the flagellar model have been developed in terms of a time unit equal to one beat cycle, a length unit equal to the length of the model, and a force unit which gives $C_L = 1.0$. Absolute values for the parameters can be obtained by multiplying by actual values for these unit quantities, as indicated in the table.

Stable movement patterns resulting from other computations are shown in Figs. 2–4. In order to conserve computing time, these computations were begun by giving the model a shape close to the final shape shown in Fig. 1, and then computing for 2½–3 beat cycles. Positions of the model at ¼-cycle intervals during the last beat cycle have been superimposed to show the final movement pattern obtained. Fig. 2 *a* illustrates the results obtained in this way using the parameters given in Table I.

TABLE I

PARAMETERS FOR THE MOVEMENT SHOWN IN FIGS. 1 AND 2 *a*

Parameters	Value	Dimensioned quantities*
Computing parameters		
Number of segments along the length of the model:	$n = 25$	
Time step:	$\delta t = 0.0625$	f^{-1}
Internal parameters for the flagellar model		
Viscous bending resistance:	$C_B = 0.00025$	$C_L S^4$
Viscous shear resistance:	$C_S = 0.012$	$C_L S^2$
Elastic bending resistance:	$E_B = 0.00001\kappa^2$	$C_L S^4 f$
Elastic shear resistance:	$E_S = 0.088\sigma^2$	$C_L S^2 f$
Active moment constant:	$m_0 = 0.0356$	$C_L S^3 f$
Time delay:	$\tau = 0.0625$	f^{-1}
Parameters of the resulting movement		
Wavelength along the flagellum:	$L = 0.61$	S
Forward swimming velocity:	$V_x = 0.10$	fS
Average power dissipation against external viscous resistances:	0.19	$C_L S^3 f^2$

* The column at the right of this table gives the dimensioned quantities which must be used with the numerical values in order to obtain dimensioned values for the parameters. Typical values for sea urchin spermatozoa (Brokaw, 1965) are: beat frequency, $f = 30$ beat cycles/sec; flagellar length, $S = 0.0042$ cm; and $C_L = 0.016$ dyne cm/sec^2.

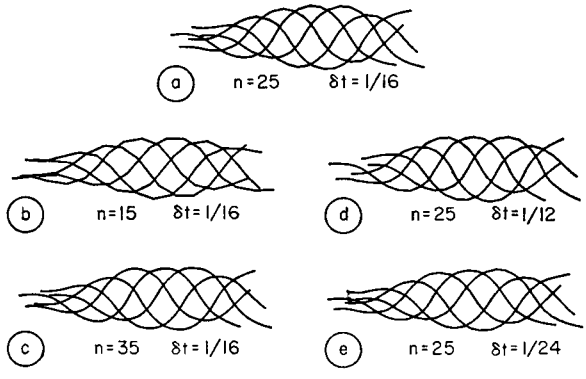

FIGURE 2 Stable movement patterns obtained from computations using the flagellar parameters listed in Table I, and various combinations of computing parameters, as indicated in the figure.

Computing Parameters

A value of 25 for n, the number of straight segments constituting the flagellar model, has been used routinely. Figs. 2 *b* and *c* show movement patterns resulting from computation with $n = 15$ and $n = 35$, respectively. All other parameters were the same as in Fig. 2 *a*, as listed in Table I. These variations in n cause no

major changes in the parameters of the resulting stable movement patterns, but the segmental character of the model becomes clearly evident when $n = 15$.

Most computations have been carried out with 16 time steps/beat cycle. This is accomplished by setting δt at 0.0625 and adjusting the value of m_0 until the wave pattern is found to repeat itself at intervals of 16 time steps. The value of δt can then be varied to carry out the computation with a different number of time steps, as in Fig. 2 *d* (12 steps/cycle) and Fig. 2 *e* (24 steps/cycle). These variations cause slight changes in the resulting movement, because any consistent error in the approximation used for forward time integration (equation 4) will effectively modify the value of the time delay τ. These errors will diminish as the number of steps per cycle is increased.

16 time steps/cycle is probably a minimum acceptable value for routine computations. The length of the time step represents a time delay in the amplitude stabilization process, and this process can become unstable if the time steps are too large. The choice of 16 time steps/cycle was dictated by the need to cover a reasonable number of beat cycles in order to reach a stable bending pattern within the computing time allotment for each run.

Flagellar Parameters

The flagellar model contains six internal parameters which determine the characteristics of its movement. These parameters are listed in Table I. The internal parameters have interrelated effects on the movement of the model, so that specification of three parameters which describe stable wave movements, such as wavelength, frequency, and amplitude, is not sufficient to determine the values of any of the internal parameters.

Stabilization of the amplitude of the movement of the model has been achieved by introducing nonlinearity in the form of cubic elastic resistances, as indicated in Table I, where E_S is proportional to the square of the amount of internal shear and E_B is proportional to the square of the curvature. The elastic parameters used to obtain the movement shown in Figs. 1 and 2 were chosen so that E_S and E_B make approximately equal contributions to stabilization of the amplitude. Effects of variations in E_S, E_B, and τ are shown in Fig. 3, and the parameters used to obtain the movements shown in Fig. 3 are given in Table II.

When the values of E_S and E_B are decreased or increased together, the amplitude of the movement changes as illustrated by Figs. 3 *a–c*. Changes in the relative values of E_S and E_B produce the results shown in Figs. 3 *d* and *e*. As E_S is decreased relative to E_B, the movement pattern becomes less uniform, probably because the shear resistance becomes dominated by the localized shear resistance which is introduced by connecting the filaments together at the base of the flagellum. With either $E_S = 0$ or $E_B = 0$, the movement is unstable when computed with 16 time steps/cycle.

Stable movements can also be obtained with less nonlinearity in the elastic re-

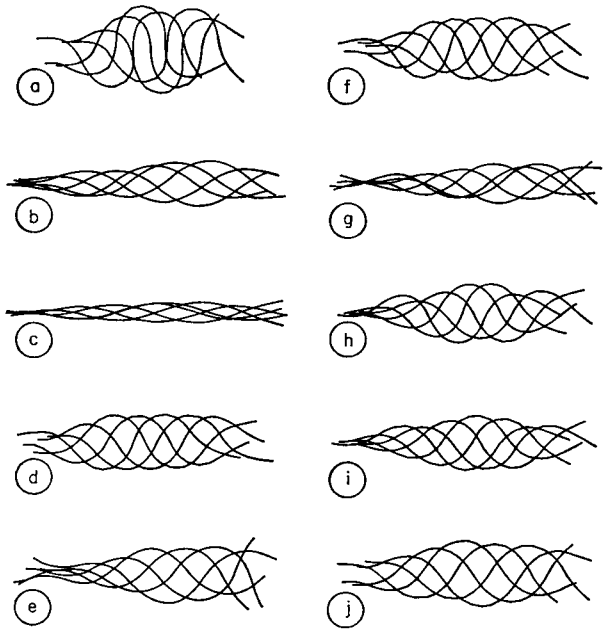

FIGURE 3 Effect of variations in elastic resistances and time delay on the stable movement patterns obtained from the flagellar model. The parameters are listed in Table II.

TABLE II

MODIFIED ELASTIC PARAMETERS USED TO COMPUTE THE MOVEMENT PATTERNS ILLUSTRATED IN FIG. 3*

Fig.	E_B	E_S
a	$0.000005\kappa^2$	$0.044\sigma^2$
b	$0.00002\kappa^2$	$0.176\sigma^2$
c	$0.00006\kappa^2$	$0.528\sigma^2$
d	$0.0000025\kappa^2$	$0.154\sigma^2$
e	$0.0000175\kappa^2$	$0.022\sigma^2$
f	0.0005	$0.088\sigma^2$
g	0.00075	$0.088\sigma^2$
h	$0.00034 + 0.0000025\kappa^2$	$0.056 + 0.022\sigma^2$
i‡	$0.0000048\kappa^2$	$0.042\sigma^2$
j§	$0.0000174\kappa^2$	$0.154\sigma^2$

* The numerical values in this table must be multiplied by the dimensioned quantities indicated in Table I to obtain absolute values.

‡ For pattern 3 *i*, the time delay τ was altered to 0.03125, and $m_0 = 0.0336$.

§ For pattern 3 *j*, $\tau = 0.1$, $m_0 = 0.0417$, and $\delta t = 0.05$. All other parameters are the same as those given in Table I.

sistances. The movements shown in Figs. 3 *f* and *g* were obtained by replacing the cubic elastic bending resistance (E_B) with linear elastic bending resistance. The movement shown in Fig. 3 *h* was obtained by replacing three-fourths of both cubic elastic resistances with linear elastic resistances.

The values of τ and m_0 are also involved in determining the amplitude of the movements. With $\tau = 0.0625$, as in all the computations considered up to this point, the time delay introduces a phase angle of 22.5° between $-\kappa$ and m, so that a component of active moment with a peak amplitude equal to 38% of the peak total active moment will occur in phase with κ, and tend to increase the curvature of the bends. This component of active moment is balanced by moments resulting from the elastic resistances. If the time delay is reduced to half this value, an adjustment of m_0 by a factor of cos 22.5°/cos 11.25° should maintain the same component of active moment to balance the viscous moments, and an adjustment of the elastic resistances by a factor of tan 11.25°/tan 22.5° should cause the amplitude to stabilize at the same value. The result of these changes is illustrated in Fig. 3 *i*. Increasing τ to 0.10, and making adjustments to m_0 and the elastic resistances, led to the result shown in Fig. 3 *j*. The small differences between these patterns and that in Fig. 2 *a* may reflect the fact that inaccuracy introduced by the approximate nature of equation 4 will alter the effective value of the time delay τ.

Although, after making appropriate adjustments, there is little difference in the stable movement patterns obtained with different values of τ, there are significant differences in the rate of approach to the stable movement pattern. For instance, the movement shown in Fig. 3 *j* was obtained from an experiment in which the initial position of the model was the same as position 1 of Fig. 1. After a time equivalent to 1½ cycles, the movement with $\tau = 0.10$ had built up to a pattern with an amplitude equivalent to that reached after 2½ cycles (position 41 of Fig. 1) when $\tau = 0.0625$. The pattern shown in Fig. 3 *j* covers the period from 2½–3½ cycles after initiation. It has reached an apparently stable amplitude, while the amplitude in Fig. 1 is still increasing after 2½ cycles. An even longer time was required for amplitude stabilization in the case where $\tau = 0.03125$ (Fig. 3 *i*).

The value of the time delay τ and the degree of nonlinearity in the elastic resistances appear to influence the transient response and the stability of the model, rather than the parameters of the stable movement. Determination of values for the time delay, and for the elastic resistances of flagella, may require information from studies of transient phenomena or from studies of the effect of variations in beat frequency on the amplitude.

The wavelength of the movement is primarily controlled by the values of C_B and C_S relative to C_L. These viscous parameters will also influence the frequency, so that when the internal viscous resistances are altered, m_0 must be adjusted to maintain 16 time steps/cycle. The elastic resistances must also be altered to compensate for the changes in m_0 and wavelength in order to maintain a relatively constant amplitude for the bending waves.

Some effects of variations in the internal viscous shear resistance C_S are illustrated in Figs. 4 *a* and *b*. Since a 12% decrease in m_0 was sufficient to maintain a constant frequency when C_S was decreased from 0.012 (Fig. 2 *a*) to 0.004 (Fig.

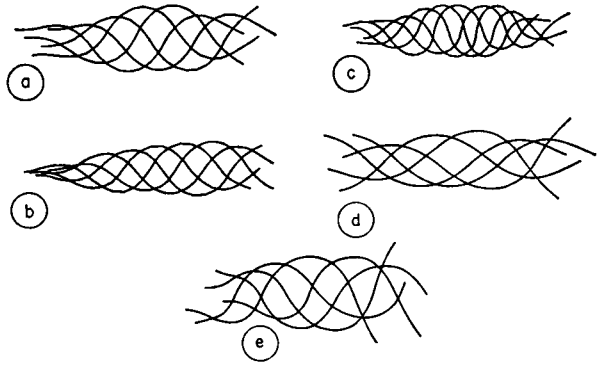

FIGURE 4 Effects of variations in viscous resistances are shown by the stable movement patterns in *a–d*. The dimensionless portions of the flagellar parameters are:

	a	*b*	*c*	*d*
C_B	0.00025	0.00025	0.0000625	0.0010
C_S	0.004	0.036	0.004	0.036
E_B	$0.000009\kappa^2$	$0.0000135\kappa^2$	$0.0000005\kappa^2$	$0.0001\kappa^2$
E_S	$0.08\sigma^2$	$0.12\sigma^2$	$0.040\sigma^2$	$0.25\sigma^2$
m_0	0.0314	0.0483	0.0112	0.112

Other parameters are those listed in Table I, except that $n = 32$ for *d*. Pattern *e* was obtained with a nonlinear form for the active process, as described in the text, and $n = 35$. All other parameters are the same as those listed in Table I.

4 *a*), the value of C_S used to obtain the movements in Figs. 1–3 only accounts for about 18% of the total viscous resistance. As shown in Figs. 4 *c* and *d*, changes in C_B produce much greater changes in the wavelength of the movement. Since changes in C_B and C_S change the wavelength in opposite directions, it is possible to find combinations of relatively low values of C_B and C_S, or relatively high values of C_B and C_S, which will produce the same wavelength. The values of C_B and C_S used in Figs. 1–3 were chosen so that the effect of changes in external viscosity on the propagation velocity would be comparable with experimental observations. An increase in external viscosity by a factor of three caused a 37% decrease in propagation velocity with the movement parameters used for Figs. 1 and 2. Integration of the work done against viscous forces indicated that with these parameters, about 30% of the viscous work was done against the external viscosity, and 70% against the internal viscous resistances.

Fig. 4 *e* illustrates another type of variation in the internal parameters which has not yet been explored thoroughly. In this case, a nonlinear function was used for $m(\kappa)$, instead of the linear relationship used in all the other computations. This nonlinear function was introduced by giving m_0 a value of 0.52, but placing an upper limit of 0.26 on the absolute value of $m(\kappa)$. This limit comes into effect by the time that the curvature has reached about 10% of its peak value, so that effectively this matches the situation where the active process can exist in only two states: either fully activated in one direction, or fully activated in the other direction.

There is only a small transition region between these two states, so this represents an extreme form of a nonlinear active process. As shown in Fig. 4 *e*, stable movements can also be obtained with this nonlinear form of control process. The wave parameters are obviously different from those obtained with a linear active process, and computations with modified internal parameters frequently led to unstable movements; however, it is clear that the introduction of some nonlinearity into the active process will still permit the generation of realistic movements.

The Shape of the Bent Regions

More detailed information about the shape of the bending waves can be obtained by examining curves which show the curvature κ and rate of change of curvature $\dot{\kappa}$ as functions of position s along the length of the flagellar model. Two sets of these curves are shown in Fig. 5. The curves in Fig. 5 *a* are taken from the computations which led to the patterns shown in Fig. 2 *c*, with $n = 35$. These curves are typical of the curves obtained in all the computations with a linear $m(\kappa)$. The curves in Fig. 5 *b* are taken from the computations with a nonlinear $m(\kappa)$ which produced the pattern shown in Fig. 4 *e*, again with $n = 35$.

The curvature varies more or less sinusoidally along the length of the model in the results obtained with a linear $m(\kappa)$, as in Fig. 5 *a*. The resulting wave form would therefore be very similar to that known as a "sine-generated" wave (cf. Brokaw et al., 1970). With the nonlinear $m(\kappa)$, the values of curvature are more constant in the regions of bending, and the values for the rate of bending are more sharply peaked in the regions between bends. The resulting wave form would more closely approach those described as being constructed of circular arcs and straight lines (Brokaw, 1965). Either of these wave forms is very close to those actually observed on flagella. More accurate methods for measuring the curvature of a flagellum from photographs are required in order to use this information to characterize the active process.

Uniformity of Propagation

The curve shown in Fig. 6 was constructed from the results of the computation illustrated in Figs. 2 *c* and 5 *a*. Using the output curves which show the curvature as a function of position along the flagellum, as in Fig. 5 *a*, the position of each point where the curvature crosses the s axis was measured. These points correspond to inflection points in the wave form. Their positions were plotted in Fig. 6 as a function of time in the beat cycle, to show the progression of a particular inflection point along the flagellar model. This result may be compared with data from photographs of sea urchin sperm flagella, shown in text figures 2 and 4 of Brokaw (1970). In those figures, similar curves were constructed to show the progression along the flagellum of bending and unbending points at the ends of circular bent regions.

The velocity of bend propagation in the mid-region of the model is at least as

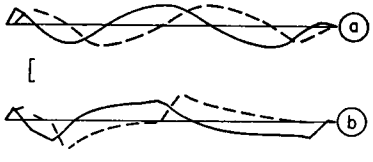

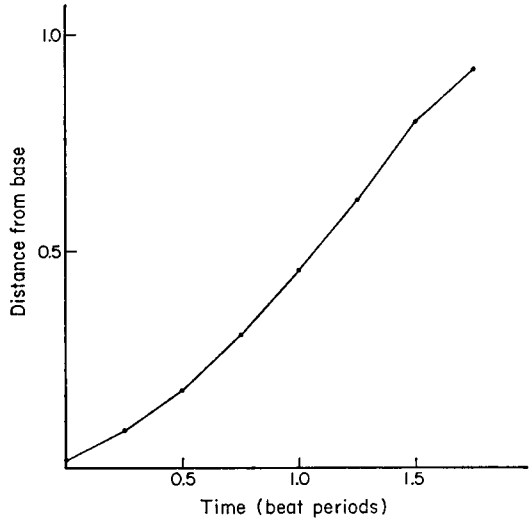

FIGURE 5

FIGURE 6

FIGURE 5 Values of curvature κ (solid curves) and rate of change of curvature $\dot{\kappa}$ (broken curves) as functions of position along the length of the model. The curves in *a* are from the computation of Fig. 2 *c* and the curves in *b* are from the computation of Fig. 4 *e*. The vertical scale marker indicates a curvature of 10 radians/flagellar length, or a rate of change of curvature of 20π radians/flagellar length per beat cycle.

FIGURE 6 The curve shows the position of an inflection point between bends as a function of time. The points were obtained from the computation of Fig. 2 *c*.

uniform as that indicated by the experimental data of Brokaw (1970). In both cases the velocity decreases slightly near the distal end of the flagellum. The bend propagation velocity in the basal region of real flagella is initially low, and then increases rapidly to its final value, while the bend propagation velocity of the model increases only slowly in the basal region. In neither case is there any indication of a decreased propagation velocity in the mid-region of the flagellum, where the bending moments resulting from viscous resistances are highest.

DISCUSSION

The generation of stable patterns of propagated bending waves by the computer model confirms that the mechanism for bend propagation by a sliding filament model for flagella, presented earlier (Brokaw, 1971), is an adequate explanation for flagellar bend propagation. In addition, the computer model demonstrates that the assumptions of this mechanism are also sufficient to explain the rhythmic initiation of bends at the base of a flagellum. In contrast to other suggested mechanisms for flagellar bend propagation (Brokaw, 1966 *a*; Lubliner and Blum, 1971; Rikmenspoel, 1971), rhythmic bend initiation is an intrinsic property of the flagellum, rather than the result of the activity of a special control oscillator located at

the base of the flagellum. Oscillation results from the presence of phase-shifted feedback between bending and the active process. The phase shift is inherent in the properties of the sliding filament mechanism (Brokaw, 1971) and does not depend on the presence of a time delay.

The bending wave patterns generated by the model can, by proper selection of internal parameters, match the values of wavelength, frequency, and amplitude shown by real flagella. The detailed shape of the bending waves, and the uniformity of bend propagation velocity, are also similar to the movements of real flagella; however, a major difference between the movement obtained from the model and the bending wave patterns seen in photographs of sea urchin sperm flagella (Brokaw, 1965, 1970) is found near the basal end of the model. As indicated in Fig. 6, the inflection points between bends show only a relatively slow increase in propagation velocity near the basal end of the model, and the curvature of bends in this region of the model is similar to, or less than, that found on the rest of the model. With real flagella, the ends of a bent region propagate very slowly near the base of the flagellum, and then accelerate rapidly to their terminal velocity (Brokaw, 1970). As a consequence, the curvature of the flagellum in bent regions near its base is usually much greater than in other regions of the flagellum. It has been impossible to obtain this type of bend initiation behavior from the model with any combination of internal parameters having constant values along the entire length of the model. Further simulation experiments, using a modified model which allows the internal parameters to vary along the length of the model, will be required to seek an explanation for the bend initiation behavior of real flagella, and to explore the suggestion that the presence of an inactive "terminal piece" at the distal end of a flagellum may improve the regularity of its movements (Brokaw, 1965, 1971). These modifications of the model, and modification to include a head attached to the basal end of the model, may make it possible to generate movements which precisely match the movements of real spermatozoa. It will then be possible to make a detailed comparison between the response of the model and the response of real spermatozoa to changes in external viscosity, which may provide sufficient information to assign absolute values to the internal parameters of the flagellar model.

To obtain stable movement patterns from the flagellar model, it has been necessary to add two features to the model in addition to those discussed in the earlier paper (Brokaw, 1971) describing the mechanism for the control of bend propagation. It has been necessary to include nonlinear elastic resistances in order to stabilize the amplitude of the movement, and to include internal viscosity in order to stabilize the wavelength of the movement.

The stabilization of amplitude by a balance between nonlinear elastic resistances and a time-delayed component of the active bending moment is straightforward; however, there may be other factors which contribute to, or are responsible for, the amplitude stabilization of the movements of real flagella. Further investigation

will be required to obtain evidence about whether nonlinear elastic resistances are responsible for amplitude stabilization of real flagella.

The relationship between internal viscosity and the stabilization of wavelength is a novel and unpredicted result of the computer simulation of flagellar movement, and requires a more extensive discussion. In the course of developing the model, an attempt was made to find values of $\dot{\kappa}(s)$ from a set of equations obtained by balancing only the external viscous bending moment (M_v) and the active bending moment (M_a). These solutions did not have the form required for uniform bending wave propagation. Instead, $\dot{\kappa}(s)$ had very high values, which alternated in sign at each joint. In effect, the model was attempting to produce movements with the smallest allowable wavelength. The values of $\dot{\kappa}(s)$ were also found to increase at each end of the model. This increase probably results from the fact that as the ends of the model are approached, M_v approaches 0 more rapidly than any simple distribution of M_a, which suggested, correctly, that an internal viscous resistance might be needed to stabilize the movement.

The effect of internal viscous resistance on the wavelength can be considered in terms of the equations for small amplitude sinusoidal movement, which neglect any distinction between distances measured along the flagellum and along the x axis, and neglect any effects introduced by the ends of the flagellum. The movement can then be represented by

$$y = b \cos 2\pi(ft - x/\lambda) \text{ or } \kappa = -\kappa_0 \cos 2\pi(ft - x/\lambda), \tag{29}$$

as in Brokaw (1971), with κ_0 representing the peak magnitude of the curvature. The component of active bending moment in phase with M_v is then obtained by integrating equation 1, with κ given by equation 29, to give:

$$M_a = m_0 \kappa_0(\lambda/2\pi) \cos 2\pi\tau \sin 2\pi(ft - x/\lambda). \tag{30}$$

Using equation 29, and equations 14 and 15 of Brokaw (1971), and introducing terms for the internal viscous moments, gives the following expression for the total viscous bending moment:

$$M_V = -2\pi f\kappa_0[C_N(\lambda/2\pi)^4 + C_S(\lambda/2\pi)^2 + C_B] \sin 2\pi(ft - x/\lambda). \tag{31}$$

The active and viscous bending moments can have equal magnitudes, to satisfy equation 3, for certain values of f and λ. In Fig. 7, the active and viscous bending moments are illustrated as functions of wavelength λ. There will be one value of frequency f_0 which gives only one point of intersection between the two functions (point B in Fig. 7). No frequency greater than f_0 is possible. At lower frequencies, there will be two points of intersection, and therefore two values of λ at which $M_a = -M_v$.

Regardless of the starting conditions, the movements obtained from computa-

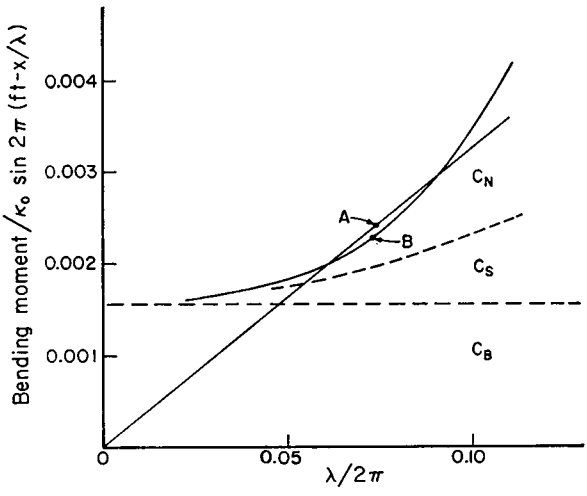

FIGURE 7 Effect of wavelength on the balance between active and viscous bending moments, for small amplitude wave movement. The viscous bending moment, indicated by the solid curve, was obtained from equation 31, with C_N = 1.8, C_S = 0.012, and C_B = 0.00025. The area under this curve is partitioned by broken lines which indicate the contributions of the three viscous resistances to the total viscous bending moment. The solid straight line indicates the active bending moment, and has a slope of $m_0 \cos 2\pi\tau$, with m_0 = 0.0356. Point *A* corresponds to the result obtained from the computation of small amplitude wave movement in Fig. 3 *c*. Point *B* indicates the predicted wavelength if the beat frequency reaches its maximum possible value.

tions with the flagellar model have been found to stabilize at a frequency close to f_0 and to have a wavelength close to that predicted by the above discussion. The curves shown in Fig. 7 were obtained using the values for the external and internal viscous parameters used for all the computations in Figs. 1–3, and a value of 0.0356 for m_0. This value of m_0 is only slightly different from the value of 0.0343 which would cause the two curves to intersect at point *B*, corresponding to a wavelength of 0.46 *S*. The movement pattern shown in Fig. 3 *c*, which has a very small amplitude, has a frequency and wavelength shown by point *A* which are nearly indistinguishable from the predicted values. At larger amplitudes, where equation 31 becomes less accurate, there is little change in frequency, but the wavelength of the stable movement pattern increases.

Stabilization of the frequency of the movement close to the maximum frequency f_0 implies that the model tends to maximize its frequency, rather than beating at a frequency which is appropriate for an initially determined wavelength. A tendency to maximize the beat frequency might result from the fact that the frequency of bend initiation has to be established near the basal end of the flagellum, where the viscous bending resistances are always less than in the mid-region of the flagellum; however, this explanation has not been verified.

An internal viscous shear resistance is a reasonable addition to a flagellar model,

because it will be similar in effect to an active process which generates less moment during active sliding. Indications of this type of behavior, which resembles the force-velocity behavior of muscle (Hill's equation), have been found with some flagella (Brokaw, 1966 *b*) and cilia (Yoneda, 1962). A more exact model for an active process incorporating this type of behavior should receive further study.

Most of the internal viscosity required to stabilize the movement of the model, however, is a viscous bending resistance rather than a viscous shear resistance. Examination of equations 30 and 31 and Fig. 7 indicates that the combination of $C_B = 0$ and a tendency to maximize the beat frequency will cause the wavelength of the movement to approach 0. The values of internal viscous resistances used to compute the movements in Figs. 1 and 2 are such that only about 30% of the work done by the flagellum is done against the external viscous resistance, and most of the remainder is dissipated against the internal viscous bending resistance. Although this appears to be a rather inefficient arrangement, it is consistent with the experimental observation that real flagellar movements are relatively insensitive to the external viscosity (Brokaw, 1962, 1966 *b*). For example, a threefold increase in external viscosity, which caused a 37% decrease in the velocity of bend propagation by the model, caused decreases of 32–40% in the velocity of bend propagation by sperm flagella (Brokaw, 1966 *b*).

Future work with this computer model should include a more extensive investigation of the effects of changes in external viscosity, investigation of more detailed models for the active process, attempts to modify the model to generate ciliary bending patterns, and exploration of the synchronization between two or more interacting models.

Most of this work was carried out in the Department of Zoology at Cambridge University.
I am grateful to the members of that department for their hospitality, and to the Cambridge University Computer Laboratory for generous provision of computer time.
I am grateful to the John Simon Guggenheim Foundation for fellowship support.

Support for this work has also been received from the National Science Foundation (GB 32035).

Received for publication 29 October 1971 and in revised form 28 January 1972.

REFERENCES

BROKAW, C. J. 1962. *In* Spermatozoan Motility. D. W. Bishop, editor. American Association for the Advancement of Science, Washington, D.C. 269–278.
BROKAW, C. J. 1965. *J. Exp. Biol.* **43**:155.
BROKAW, C. J. 1966 *a*. *Nature (London)*. **209**:161.
BROKAW, C. J. 1966 *b*. *J. Exp. Biol.* **45**:113.
BROKAW, C. J. 1970. *J. Exp. Biol.* **53**:445.
BROKAW, C. J. 1971. *J. Exp. Biol.* **55**:289.
BROKAW, C. J., S. F. GOLDSTEIN, and R. L. MILLER. 1970. Comparative Spermatology. Academic Press, Inc., New York. 475–486.
COX, R. G. 1970. *J. Fluid Mech.* **44**:791.
GRAY, J., and G. J. HANCOCK. 1955. *J. Exp. Biol.* **32**:802.
LUBLINER, J., and J. J. BLUM. 1971. *J. Theor. Biol.* **31**:1.

MACHIN, K. E. 1958. *J. Exp. Biol.* **35**:796.
RIKMENSPOEL, R. 1971. *Biophys. J.* **11**:446.
SATIR, P. 1965. *J. Cell Biol.* **26**:805.
SATIR, P. 1968. *J. Cell Biol.* **39**:77.
YONEDA, M. 1962. *J. Exp. Biol.* **39**:307.

APPENDIX I

Coefficients for Evaluation of the External Viscous Bending Moment

The flagellum is approximated by n straight segments, connected by $n - 1$ joints at which values of κ and $\dot{\kappa}$ are defined. $\dot{\kappa}(j)$ represents the value of $d\kappa/dt$ at the jth joint. The total length of the flagellum is used as the unit of length, so that the length of each segment of the model is $1/n$. An x, y coordinate system is defined with its origin at the basal end of the flagellum and an angle $\alpha(1)$ between the x axis and the first segment of the model. The angle between the x axis and the jth segment is then

$$\alpha(j) = (1/n) \sum_{k=2}^{j} \kappa(k - 1) + \alpha(1). \tag{32}$$

The x, y coordinates of the jth joint are given by

$$x(j) = (1/n) \sum_{k=1}^{j} \cos \alpha(k) \tag{33}$$

and

$$y(j) = (1/n) \sum_{k=1}^{j} \sin \alpha(k). \tag{34}$$

The movement of the jth segment can be specified by the x and y velocities of its basal end, represented by $\dot{x}(j - 1)$ and $\dot{y}(j - 1)$, respectively, and its angular velocity relative to the x axis, represented by $\dot{\alpha}(j)$. These quantities can be found from equations similar to equations 18–20 of Brokaw (1970):

$$\dot{\alpha}(j) = -W + (1/n) \sum_{k=2}^{j} \dot{\kappa}(k - 1), \tag{35}$$

where W represents the angular velocity of the basal end of the flagellum as defined in Brokaw (1970), so that $W \equiv -\dot{\alpha}(1)$.

$$\dot{x}(j) = V_x + Wy(j) - (1/n) \sum_{k=1}^{j-1} [y(j) - y(k)]\dot{\kappa}(k) \tag{36}$$

and

$$\dot{y}(j) = V_y - Wx(j) + (1/n) \sum_{k=1}^{j-1} [x(j) - x(k)]\dot{\kappa}(k), \tag{37}$$

where $V_x \equiv \dot{x}(0)$ and $V_y \equiv \dot{y}(0)$ are the velocities of the basal end of the flagellum.

For convenience, the following functions of C_N, C_L, and $\alpha(j)$ will be defined:

$$\begin{aligned} D(j) &= C_L \cos^2 \alpha(j) + C_N \sin^2 \alpha(j), \\ E(j) &= C_L \sin^2 \alpha(j) + C_N \cos^2 \alpha(j), \\ G(j) &= (C_N - C_L) \sin \alpha(j) \cos \alpha(j). \end{aligned} \tag{38}$$

The x and y components of the force in the flagellum at the jth joint are given by equations similar to equations 5 and 6 of Brokaw (1970), expressed as a summation along the length rather than an integral:

$$F_x(j) = F_x(0) - (1/n) \sum_{k=1}^{j} \left[\dot{x}(k-1)D(k) - \dot{y}(k-1)G(k) - \frac{1}{2} C_N(1/n)\dot{\alpha}(k) \sin \alpha(k) \right], \tag{39}$$

$$F_y(j) = F_y(0) - (1/n) \sum_{k=1}^{j} \left[\dot{y}(k-1)E(k) - \dot{x}(k-1)G(k) + \frac{1}{2} C_N(1/n)\dot{\alpha}(k) \cos \alpha(k) \right]. \tag{40}$$

The moment at the jth joint is then given by an equation similar to equation 7 of Brokaw (1970), again expressed as a summation along the length rather than an integral, and containing additional terms to give an accurate computation when n is small:

$$\begin{aligned} M_v(j) = M_v(0) + (1/n) \sum_{k=1}^{j} \Big\{ & F_y(k-1) \cos \alpha(k) \\ & - F_x(k-1) \sin \alpha(k) - \frac{1}{2} C_N(1/n) \left[\dot{y}(k-1) \cos \alpha(k) \right. \\ & \left. - \dot{x}(k-1) \sin \alpha(k) \right] - (C_N/6)(1/n)^2 \dot{\alpha}(k) \Big\}. \end{aligned} \tag{41}$$

After insertion of the expressions for $\dot{\alpha}(j)$, $\dot{x}(j)$, and $\dot{y}(j)$ into these equations, $M_v(j)$, $F_x(j)$ each become functions of V_x, V_y, W, and the values of $\dot{\kappa}$ at the first $j-1$ joints. These functions can then be rewritten in the form of equation 5, and the values of $A(j, k)$ can be obtained by the summation processes indicated in equations 39–41.

The result is a matrix of $A(j, k)$ coefficients for $n + 2$ equations containing V_x, V_y, W, and $n - 1$ values of $\dot{\kappa}$ as variables.

APPENDIX II

Evaluation of a Proposal for Simultaneous Activation of Active Sliding

A computation of the distribution of bending moment along a swimming flagellum has also been carried out by Rikmenspoel (1971). His results differ significantly from those of Brokaw (1970), although both were based on the same type of data. Rikmenspoel concludes that the distribution of bending moment required to generate flagellar waves can be produced by a

sliding filament process if the active elements are activated simultaneously along the length of the flagellum. Each active element goes through a cycle of activity in which it produces a shear or shear moment in alternate directions, and all elements along the length oscillate in the same phase.

Rikmenspoel's suggestion can be evaluated easily with the computer model described in his paper, by simply replacing equation 1 with:

$$dM_a/ds = -m_0 \cos 2\pi ft, \qquad \text{for } 0 \leq s \leq 1. \tag{42}$$

dM_a/ds is therefore independent of s or κ, and varies sinusoidally with time. A typical result obtained from computation with this specification of the active process is shown in Fig. 8.

FIGURE 8 Movement of a sliding filament flagellar model with simultaneous activation along the length. The internal parameters are $C_B = 0.00025$, $C_S = 0$, $E_B = 0.003$, $E_S = 0$. Five successive positions are shown, which cover a half-cycle of movement at $\frac{1}{8}$-cycle intervals.

The stable movement pattern consists of bends which are initiated near the base of the flagellar model, but decrease rapidly in amplitude as they propagate along the length. These waves are very similar to those computed by Machin (1958) for the case of a passive elastic flagellum driven by an oscillator at its base.

Rikmenspoel's suggestion is attractive, because it implies that no control mechanism is required to maintain phase differences between the active elements along the length of a flagellum. Computations with the model, however, indicate that Rikmenspoel's suggestion does not provide a sufficient basis for the propagation of bending waves of sustained amplitude, and indicate that a local control mechanism, similar to the one originally suggested by Machin (1958) and applied to a sliding filament model by Brokaw (1971 and in this paper), is necessary to explain the propagation of flagellar waves.

Several differences between the methods used for analyzing flagellar bending moments by Rikmenspoel (1971) and by Brokaw (1970 and this paper) may be responsible for the different conclusions reached about the mechanism for the control of the active process. Rikmenspoel does not assume as a boundary condition that $M_v = 0$ at the base of the flagellum, but instead introduces "the observed motion" as a boundary condition at the base. It seems more likely that for a free-swimming flagellum the boundary conditions for M_v must be the same at each end of the flagellum, and that the observed motion of the base should form part of the solution for the movement, rather than a boundary condition. Other errors may enter into Rikmenspoel's computations as a result of his use of small amplitude equations to analyze the data from large amplitude flagellar movements.